Acta metall. mater. Vol. 41, No. 12, pp. 3401–3411, 1993
Printed in Great Britain.

0956-7151/93 $6.00 + 0.00

CALCULATION OF THE INTERNAL STRESSES AND STRAINS IN THE MICROSTRUCTURE OF A SINGLE CRYSTAL NICKEL-BASE SUPERALLOY DURING CREEP

L. MÜLLER, U. GLATZEL and M. FELLER-KNIEPMEIER

Institut für Metallforschung, Sekr. BH 18, Technische Universität Berlin, Straße des 17. Juni 135, 10587 Berlin, Germany

(Received 30 November 1992; in revised form 27 April 1993)

Abstract—The evolution of internal stresses and strains in the microstructure of a single crystal nickel-base alloy during annealing and during creep in [001] direction has been calculated using a visco-plastic model. Two limiting conditions are considered: an "overloading" case where the internal stresses reach the critical resolved shear stress of the whole γ' volume and an "underloading" case where the critical resolved shear stress of the γ' precipitate is reached only at distinct areas. During creep deformation a triaxial stress state evolves in the microstructure and large pressure gradients are built up. The influence of an initial coherency misfit is shown to be negligible after short times of creep. The calculations allow the prediction of flow patterns in the microstructure, creep-induced lattice parameter changes, type and arrangement of interfacial dislocations and of the dependence of the stationary strain rate on the cube or plate morphology of the γ' phase.

Zusammenfassung—Die Entwicklung von inneren Spannungen und Dehnungen in der Mikrostruktur einer einkristallinen Nickelbasislegierung während des Anlassens and während des Kriechens in [001] Richtung wurde mit einem viscoplastischen Modell berechnet. Es können zwei Grenzfälle unterschieden werden: der "Überlastfall", bei dem die inneren Spannungen größer als die kritische Schubspannung des gesamten γ' Volumens werden, und der "Unterlastfall", bei dem die kritische Schubspannung nur in bestimmten Bereichen der Ausscheidung erreicht wird. Während der Verformung baut sich in der Mikrostruktur ein dreiachsiger Spannungszustand mit hohen Druckdifferenzen auf. Der Einfluß der kohärenten Gitterfehlpassung auf das Kriechverhalten nimmt schnell ab. Die Berechnungen erlauben die Vorhersage der Fließprofile in der Mikrostruktur, von kriechinduzierten Änderungen der Gitterparameter, des Typs und der Anordnung von Grenzflächenversetzungen und der Abhängigkeit der stationären Dehnrate von der Würfel- bzw. Plattenmorphologie der γ' Phase.

1. INTRODUCTION

Modern nickel-base superalloys are strengthened by a high volume fraction of hard cuboidal γ' precipitates embedded coherently in a softer matrix.

Due to the mismatch in lattice parameters of the phases high coherency stresses build up in the microstructure. Finite element methods (FEM) have been used by several authors in order to calculate their distribution [1–8] and different experimental techniques have been applied for their measurement [9–12]. FEM calculations of the strain distribution in the microstructure were also successfully compared with neutron diffraction spectra of the lattice parameter distribution in a coherently-stressed nickel-based superalloy [12]. In addition, calculations of the strain energy stored in the γ/γ' microstructure were shown to determine the equilibrium shape of the γ' precipitates in the underformed state and under external load [3–5, 8].

2D and 3D calculations were compared in [8]. In order to compare theoretical with experimental results it is necessary to make 3D calculations [8, 12]. 2D are only useful to get a quick and qualitative survey of the stress field in the microstructure.

Calculations of the development of the internal stresses during creep deformation have so far been restricted to two-dimensional analysis and square precipitates which were not permitted to deform plastically [7].

In the present paper we will calculate the internal stress distribution and the macroscopic strain curve for cubic γ' morphology during creep deformation using the FEM-technique. Analytical results will be presented for the γ' plate morphology. The calculations were done using the parameter set of SRR99†.

Our calculations will be compared with experimental results such as lattice parameter measurements [11, 13–15], TEM investigations [16–18] and creep curves [19, 20].

2. MICROMECHANICAL MODEL

After standard heat treatment of SRR99 the γ' cuboids have a volume fraction of 70% and an edge

†SRR99 is a trademark of Rolls-Royce plc.

length of 0.5 μm [2, 21, 22]. They are coherently and periodically embedded in the matrix with a channel width of approximately 50 nm. The γ/γ' interfaces are aligned parallel to the {001} cube planes.

For the calculation a volume element containing one eighth of the γ' cube surrounded on three sides by its matrix channels is chosen. The γ and γ' materials are connected compatibly at the phase interface. The unit-cell method, the corresponding boundary conditions and the introduction of the misfit into the model are described in [1, 2, 6–8].

We will make two and three-dimensional calculations. 2D calculations allow for a quick overview over the stress distribution in the microstructure, whereas 3D calculations are necessary to obtain quantitative results. Choosing 6^2, 10^2, or 20^2 finite elements for 2D and 3^3, 4^3, 5^3 or 6^3 for 3D elements has only minor influence on the numerical results for total elongations less than 3%. The finite element meshes and the choice of finite elements were already presented in [2, 8].

Due to the small dimensions of the two phases in the superalloy, both phases deform completely different in composite as compared to bulk γ and γ' material.

From TEM results [7, 16, 17] it is known that at elevated temperatures the creep deformation starts in the matrix phase. Only at later stages of creep deformation the γ' precipitate is sheared by dislocations.

Consequently, the matrix is permitted to deform both elastically and by creep. We chose a creep power law relating the equivalent strain rate $\dot{\epsilon}_e$ with the equivalent von Mises stress σ_{Mises}

$$\dot{\epsilon}_e = A \cdot \sigma_{\text{Mises}}^n \tag{1}$$

where n is the creep exponent. The equivalent von Mises stress σ_{Mises} is defined by

$$\sigma_{\text{Mises}} = \sqrt{0.5 \cdot [(\sigma_{11} - \sigma_{22})^2 + (\sigma_{22} - \sigma_{33})^2 + (\sigma_{22} - \sigma_{11})^2] + 3 \cdot (\sigma_{12}^2 + \sigma_{23}^2 + \sigma_{31}^2)} \tag{2}$$

where σ_{ij} are the components of the stress tensor. The equivalent strain is defined according to the von Mises stress state. The γ' precipitates were allowed to deform elastically and perfect-plastically according to the von Mises yield criterion, when the local stress level reaches the γ' yield stress $\sigma_{\text{yield}}^{\gamma'}$.

Diffusion controlled morphological changes during creep or inhomogeneous deformations of the specimen are not considered.

2.1. *Input data*

The input data required for the calculations were taken from the literature concerning SRR99 or related superalloys. They are listed in Table 1.

As the value of γ' yield stress in composite is unknown we have chosen two different values for the γ' yield stress in parameter sets I and II in order to study two different deformation mechanisms, called overloading and underloading case. The exponent n is taken from a creep investigation of SRR99 [19].

The pre-exponential factor A was arbitrarily chosen to be equal to $A = 1.472 \cdot 10^{-42}\,\text{Pa}^{-4.7}$ for all model calculations.

In order to compare calculations and experiment one has to shift the creep time in such a way that the calculated creep curve has the same stationary creep rate (or approximately the same quasi-stationary creep rate) as the experimental curve. For example, using parameter set *I*, 100 normalized time units equal 430 h in a creep experiment of SRR99 at $T = 1123$ K [19] as shown in Fig. 9(a). This is the time scale for all other model calculations at 1123 K with other morphologies and other loading conditions.

Another possibility would be to choose the n and A values of the bulk matrix phase as done in [7]. The γ bulk material shows a value of $n = 4.7$, similar to the one we choose. Using the A value of the bulk matrix material one does not take into account the high creep resistance of γ material forced into small channels as discussed in [7].

Parameter set III will be used for the analytical calculations made to obtain the stationary stress state in the plate morphology after creep deformation at

Table 1. Input data used for calculations

	Parameter set I	Parameter set II	Parameter set III
Case	Overloading	Underloading	Underloading
Temperature	1123 K		1323 K
Youngs' modulus $E^{\gamma'}$ [8, 23]	108 GPa		85 GPa
Shear modulus $G^{\gamma'}$	98 GPa		85 GPa
Poissons' ratio $\nu^{\gamma'}$	0.40		0.41
Youngs' modulus E^{γ} [8, 23]	88 GPa		77 GPa
Shear modulus G^{γ}	97 GPa		87 GPa
Poissons' ratio ν^{γ}	0.40		0.41
Coherency misfit δ^{coh} [12]	−0.14% or 0 or +0.14%		−0.2%
γ' volume fraction (3D) [24]	70%		62%
γ' area fraction (2D) [2, 8]	73.5%		—
γ' yield stress $\sigma_{\text{yield}}^{\gamma'}$	650 MPa	750 MPa	>484 MPa
External load σ_{ext}	490 MPa		0 to 300 MPa
Load axis	[001]		
Creep exponent n [19]	4.7		>1
Pre-exponential factor A	$1.472 \cdot 10^{-42}\,\text{Pa}^{-4.7}$		—

$T = 1323$K. For the sake of simplicity, the elastic constants of the matrix will be used for both phases in our analytical considerations.

FEM calculations were done simulating:

(i) a long-term annealing experiment at $T = 1123$ K without external load;
(ii) tensile creep in [001] direction under a constant load of 490 MPa at $T = 1123$ K;
(iii) tensile creep in [001] direction at $T = 1323$ K for a γ' plate morphology.

In fact, scaling the time and stresses involved in the calculation according to the creep power law our results can be transformed to other temperature and load parameters.

All FEM analysis were performed using ABAQUS finite element code [25].

3. RELAXATION OF COHERENCY STRESSES DURING LONG-TERM ANNEALING

Using parameter set I (3D) but with zero external load and a coherency misfit of $\delta^{coh} = -0.14\%$ the stress and strain distributions for an annealing temperature of $T = 1123$ K have been calculated as function of time.

Plastic deformation of the matrix channels due to the coherency stress field is calculated using the power law of equation (1). The time dependence of stresses and strains will be discussed for selected points in matrix and γ' phase as depicted in Fig. 1.

As can be seen from Fig. 2(a) at the beginning of annealing the matrix channels as points A and B are highly loaded (247 MPa von Mises stress). The matrix crossing point G and the interior of the precipitate around point C are on a low von Mises stress level with 40 and 20 MPa, respectively.

During long-term annealing under zero external load the high coherency stress in the small matrix channels decrease drastically. The matrix crossing point G remains on its low level; the γ' interior on 30 MPa. At the normalized time t_{norm} of 1800 units the von Mises stress level in the whole microstructure is on the same low stress level ($\approx$25 MPa). Now the stresses decrease slowly towards zero for infinite times.

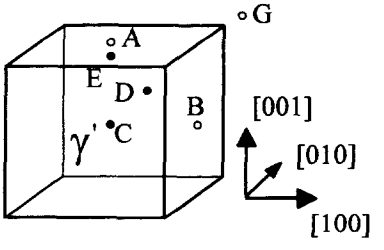

Fig. 1. γ' cube with its adjacent matrix. Open circles mark matrix points and closed circles precipitate points. Point A and point B are the midpoints of the horizontal and vertical matrix channels, respectively. Point C marks the center of the γ' cube. Point D is located near the edge of the γ' cube. Point E is on the γ' side opposite to the channel point A. Point G marks the crossing point of three matrix channels.

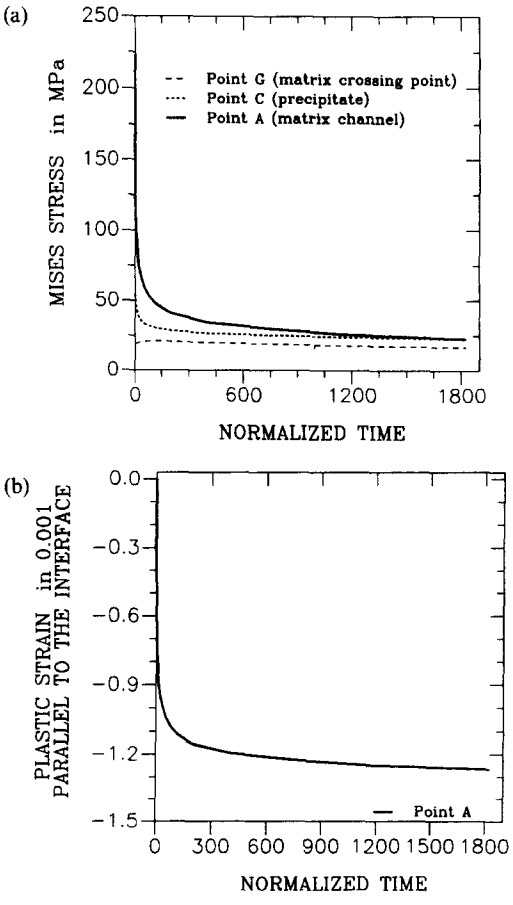

Fig. 2. (a) Evolution of von Mises stress for a cubic γ' morphology with an initial misfit value of $\delta_{coh} = -0.14\%$ over time. No external stress is applied. (b) Plastic strain built up in the matrix channel parallel to the γ/γ' interface.

The reduction of the coherency stresses is accompanied by the build-up of plastic strain in the matrix parallel to the γ/γ' interface [Fig. 2(b)]. The algebraic value of plastic strain $\delta^{parallel}$ drops quickly at the beginning. At $t_{norm} = 1800$ the plastic strain value is $\delta^{parallel} = -0.128\%$ and approaches slowly the initial coherency value $\delta^{coh} = -0.14\%$.

An interfacial edge dislocation network with a continuum distribution of infinitesimal small Burgers vectors causes such a continuum plastic strain $\delta^{parallel}$ and stresses of opposite sign to the coherency field in the narrow matrix channels. Taking into account crystallographic aspects, a quadratic dislocation network with finite Burgers vector and extra half planes inserted in the γ' phase is building up, which compensates the coherency misfit stresses [Fig. 3(a)].

4. SIMULATION OF CREEP DEFORMATION UNDER AN EXTERNAL CREEP LOAD

4.1. 2D calculation of the internal stresses

2D calculations are used for a quick survey of the stress distribution in the γ/γ' microstructure. The

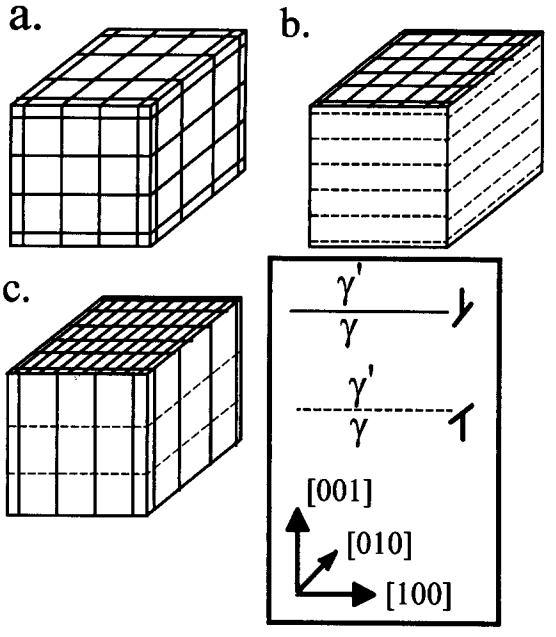

Fig. 3. Schematic depiction of interfacial dislocation networks on the faces of a γ' cube. We only consider, for the sake of simplicity, the edge component of dislocations with $\langle 001 \rangle$ line vectors lying at the γ/γ' interface. Full and broken lines correspond to line vectors where the extra half plane is inserted on the γ' and γ side, respectively. (a) During long-term annealing under no external load the initial (negative) coherency misfit can be compensated by quadratic dislocation meshes. (b) Under a tensile load in [001] direction (and no coherency misfit) interfacial dislocation networks develop which reduce the von Mises stress level in the soft matrix phase. (c) Adding the coherency dislocation meshes in (a) to the creep-induced meshes of (b) one gets the network configuration for a negative misfit alloy under [001] tensile load.

calculations were done with parameter set I for square precipitates under 490 MPa [001] tensile load (parameter set I) and plane stress condition (stresses in the third dimension are zero.)

Figure 4(a) presents the von Mises stress distribution after $t_{\text{norm}} = 8.0$ creep deformation under 490 MPa load. At this late stage of deformation the internal stress distribution is independent of the initial coherency misfit. The von Mises stress level in the matrix phase is reduced as compared to the external load of 490 MPa. The horizontal channel is on a homogeneous stress level of 440 MPa. In the vertical channel the von Mises stress level increases from 200 MPa at the midpoint of the matrix channel up to 410 MPa at the matrix crossing point. No significant stress gradient perpendicular to the γ/γ' interface is observed in the matrix. At the shaded portion the γ' material is flowing plastically as the stress level of $\sigma^{\gamma'}_{\text{yield}} = 650$ Mpa is reached. The γ' phase adjacent to the center of the horizontal matrix channel is on a stress level of 520 MPa only.

Tensile stresses have been built up parallel to the γ/γ' interfaces in order to reduce the von Mises stress level. The stress state $(\sigma_{11}, \sigma_{22}, \sigma_{33}, \sigma_{12}, \sigma_{13}, \sigma_{23})$ in the horizontal channel is approximately

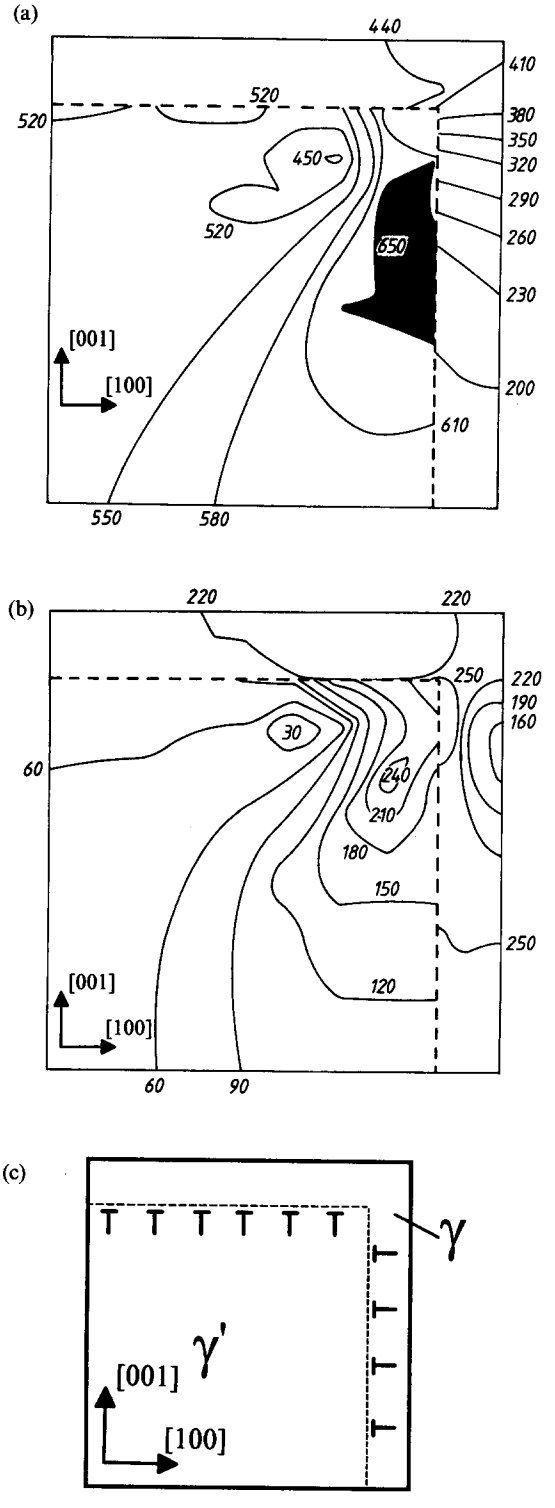

Fig. 4. 2D calculation of the von Mises stress distribution in the γ/γ' microstructure during creep deformation. Lines of constant equivalent von Mises stresses in MPa are depicted after a normalized time of 8.0. One quarter of a γ' square is shown. The broken line depicts the γ/γ' interface. (a) 490 MPa tensile load are still acting perpendicular to the upper bond. The shaded area corresponds to the deforming γ' phase. (b) Von Mises stress distribution just after removing the external load. (c) Schematic depiction of the edge dislocation network which produces the long-range residual stresses.

(250 MPa, 0, 520 MPa, 0, 0, 0). At the midpoint of the vertical channel the stress state is (120 MPa, 0, −80 MPa, 0, 0, 0).

Upon unloading the matrix relaxes to a nearly homogeneous and high von Mises stress level of about 220 MPa [Fig. 4(b)]. A complex stress state characterized by steep stress gradients remains in the γ' cube. The maximum (240 MPa von Mises stress) and minimum (30 MPa von Mises stress) are located at the neighbourhood of the γ' tip.

Residual stresses of 250 MPa tension in the horizontal channel and 200 MPa compression in the vertical channel remain parallel to the γ/γ' interfaces. Microscopically these internal stresses parallel to the interfaces are produced by interfacial edge dislocation networks as discussed in Section 3. The sign of the Burgers vector relative to the interface changes from the horizontal to the vertical channel as indicated in Fig. 4(c).

4.2. 3D calculation of the creep-induced stresses

The complex stress state in the cubic precipitate will be compared with the homogeneous stress state of the plate morphology during creep.

Two different cases are distinguished. They are denoted "overloading" and "underloading" case which differ in the γ' yield behavior.

The creep-induced stresses will be studied in Sections 4.2.1 and 4.2.2, whereas the influence of an initial coherency misfit will be examined separately in Section 4.2.3.

4.2.1. Overloading case. First, we will discuss the overloading case. In this state the external load σ_{ext} is larger than the product of the equivalent γ' yield stress $\sigma^{\gamma'}_{yield}$ and γ' volume fraction $V^{\gamma'}$

$$\sigma_{ext} > \sigma^{\gamma'}_{yield} \cdot V^{\gamma'} \tag{3}$$

γ' Cubes. At $t = 0$ under the external load of 490 MPa and $\delta^{coh} = 0$ the elastic stiffer γ' phase takes approximately 510 MPa, the horizontal matrix channel 460 MPa and the vertical channel 420 MPa [Fig. 5(a)]. Then the von Mises stress in the horizontal and vertical channel decreases rapidly up to a stationary value of ≈ 135 MPa. The γ' precipitate starts flowing at Point D near the vertical channel and the γ' tip. The flow behavior of the γ' cube is similar to that of the γ' square in 2D where the maximum von Mises stress is located near the vertical channel and the γ' tip. As soon as the von Mises stress has reached the γ' yield stress of 650 MPa, the whole γ' precipitate is deforming plastically.

Figure 5(b) presents the principal stresses in the horizontal and vertical channels during creep deformation. In the horizontal channel a triaxial tensile stress state has built up. Finally, the stress component perpendicular to the γ/γ' interface is nearly equal to the γ' yield stress of 650 MPa, whereas the stress components parallel to the γ/γ' interface are equal to the external load of 490 MPa. In the vertical channel the stress component parallel to the load axis decreases rapidly to a stationary amount of 50 MPa tension. The two other stress components are on a low compressive stress load of approximately 50 and 70 MPa, respectively.

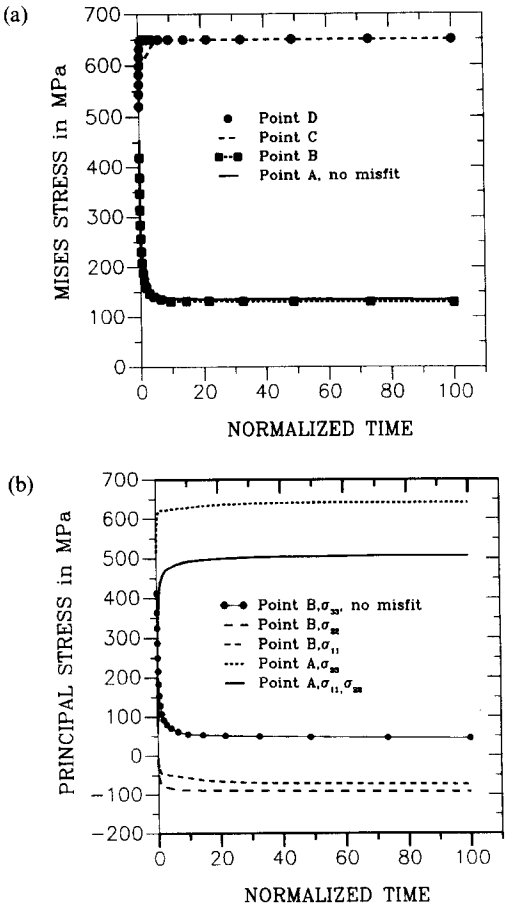

Fig. 5. (a) Evolution of the von Mises stress within the cubic γ' microstructure over time under overloading condition (parameter set I, $\delta^{coh} = 0$). Note that the precipitate regions C (precipitate center) and the edge point D start flowing at different times. (b) Evolution of the principal stresses in the horizontal (point A) and vertical channel (point B). No significant shear stresses are observed in both points.

The edge dislocations which produce these internal stress fields are displayed in Fig. 3(b). The networks in the horizontal channels have quadratic meshes, whereas in the vertical channel the arrangement consists of parallel dislocations with line vectors perpendicular to the load axis. The extra half planes are situated in the γ' phase at the horizontal channels and in the matrix at the vertical channels.

The different triaxial stress states developed during creep deformation result in a large stationary pressure gradient from the vertical towards the horizontal channel

$$p_{vert} - p_{horiz} \approx 566 \text{ MPa}. \tag{4}$$

γ' Plate morphology. A γ' plate morphology, as shown in Fig. 6, is used to simulate the microstructure that is known as γ' rafting.

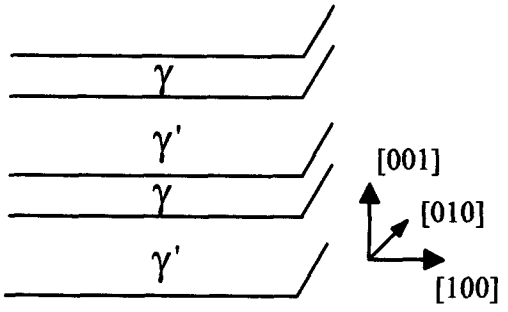

Fig. 6. Plate morphology. Alternating plates of γ and γ' phases are infinitely extended in [010] and [100] directions.

For the plate morphology the stationary stress state after creep deformation is obtained taking into account that the soft matrix tries to lower its von Mises stress level. Equilibrium conditions for the stress field were given in [8, 12, 22]. Due to the symmetry the stresses are homogeneously distributed in γ and γ' plates, respectively. In the plate morphology the build-up of shear stresses is not supported [8, 12, 22].

During a tensile creep test tension stress parallel to the interface is built up in the matrix plate, whereas the corresponding compressive stresses are found in the γ' plate. Consequently, the von Mises stresses in the γ' phase increase up to the yield stress of the precipitate in the overloading case.

The stationary stress state $(\sigma_{11}, \sigma_{22}, \sigma_{33})$ in both plate phases is given by:

$$\sigma^{\gamma} = \left[\frac{V^{\gamma'}}{V^{\gamma}}(\sigma^{\gamma'}_{\text{yield}} - \sigma_{\text{ext}}), \frac{V^{\gamma'}}{V^{\gamma}}(\sigma^{\gamma'}_{\text{yield}} - \sigma_{\text{ext}}), \sigma_{\text{ext}}\right] \quad (5)$$

$$\sigma^{\gamma'} = (\sigma_{\text{ext}} - \sigma^{\gamma'}_{\text{yield}}, \sigma_{\text{ext}} - \sigma^{\gamma'}_{\text{yield}}, \sigma_{\text{ext}}). \quad (6)$$

Qualitatively, the matrix plates, with their phase interfaces orientated perpendicular to the load axis, behave similar to the horizontal matrix channels of the cube morphology. Large tensile stress components are observed parallel to the phase interface. The stationary von Mises stress level in the matrix plate is given by

$$\sigma^{\gamma\,\text{plates}}_{\text{Mises}} = (\sigma_{\text{ext}} - \sigma^{\gamma'}_{\text{yield}} \cdot V^{\gamma'})/V^{\gamma} \quad (7)$$

when V^{γ} is the matrix volume fraction. For parameter set I we obtain $\sigma^{\gamma\,\text{plates}}_{\text{Mises}} \approx 116$ Mpa which is just smaller than the von Mises stress $\sigma^{\gamma\,\text{cube}}_{\text{Mises}} \approx 135$ MPa of the matrix channel in the cube morphology.

4.2.2. Underloading case. Now we will discuss the deformation in underloading condition which is defined by

$$\sigma_{\text{ext}} < \sigma^{\gamma'}_{\text{yield}} \cdot V^{\gamma'}. \quad (8)$$

The calculations were performed with parameter set II with a γ' yield stress of 750 MPa. The coherency lattice mismatch was considered to be zero.

γ' Cubes. The von Mises stress in the matrix channels and the cube interior decreases rapidly towards zero as depicted in Fig. 7.

The plastic deformation of the γ' precipitate begins at Point D. But then the stress level in Point D decreases below the γ' yield value of 750 MPa and other parts of the γ' precipitate deform plastically, e.g. point E after $t_{\text{norm}} \approx 3 \cdot 10^5$. The stress level in the centre of the γ' cube increases rapidly up to 700 MPa, but then drops down to 600 MPa. The average von Mises stress level of the γ' precipitate is approximately 700 MPa. Consequently, only distinct parts of the γ' precipitate are deforming at the same time.

The principal stress state in the horizontal and vertical matrix channels approaches $\sigma_{\text{horz}} \approx 650$ MPa (1, 1, 1) and $\sigma_{\text{vert}} \approx (-70\text{ MPa}, -74\text{ MPa}, -64\text{ MPa})$, respectively. The stationary pressure difference between the vertical and horizontal channel is given by

$$p_{\text{vert}} - p_{\text{horiz}} \approx 720\text{ MPa} < \sigma^{\gamma'}_{\text{yield}}. \quad (9)$$

γ' Plate morphology. γ' plates do not flow under underloading conditions. The stationary stress state in the matrix and γ' plate is $\sigma_{\text{ext}} \cdot (1, 1, 1)$ and $\sigma_{\text{ext}} \cdot (-V\gamma/V\gamma', -V\gamma/V\gamma', 1)$ respectively.

4.2.3. Relaxation of coherency stresses under an external load. Now we study how initial coherency stresses influence the creep behavior of a specimen. The calculations were done with parameter set I and different coherency misfit values.

Now we look at the von Mises stress distribution for different coherency misfit values at $t_{\text{norm}} = 0$ under the external load of 490 MPa (Fig. 8). For $\delta = -0.14\%$ and $\delta = 0$ the von Mises stresses are larger in the horizontal channel with 680 and 460 MPa than in the vertical channel with 560 and 420 MPa, respectively. For $\delta = +0.14\%$ the situation is vice versa. The von Mises stress in the horizontal channel is 240 MPa vs 360 MPa in the vertical channel.

The von Mises stresses in the matrix phase coincide after a short time $t_{\text{norm}} \approx 0.5$ for different coherency values. The misfit stresses in the horizontal and

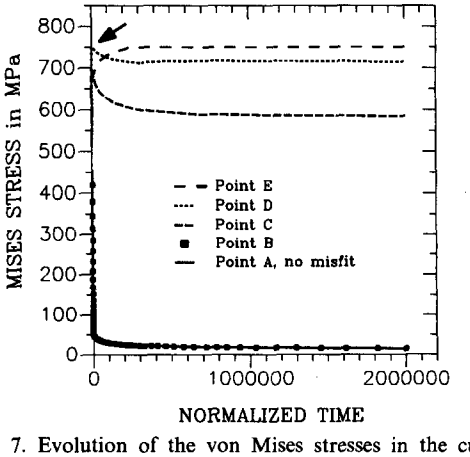

Fig. 7. Evolution of the von Mises stresses in the cubic morphology over time in underloading conditions. The arrow indicates that during a small time interval the γ' phase is flowing at point D. Point E starts flowing at a later stage of deformation.

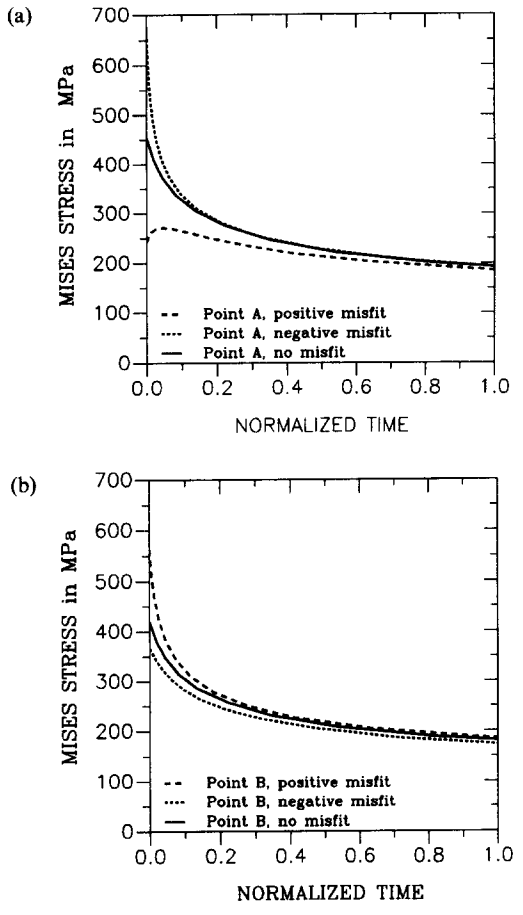

Fig. 8. Variation of the von Mises stress (a) in the horizontal and (b) in the vertical channel with different initial coherency misfit values (parameter set I, $\delta^{coh} = -0.14\%, 0, 0.14\%$) over the first normalized time unit. The curves coincide after the first normalized time unit.

vertical channel have nearly the same value of approximately 190 MPa.

Consequently, one would predict that for alloys with negative misfit the deformation should start in the horizontal matrix channels. At a later stage the deformation should also spread into the vertical channels.

During creep deformation under an external load of 490 MPa the coherency stresses are compensated approximately 1000 times faster than under zero load [compare Fig. 2(a) with Fig. 8]. The stationary stress state during creep deformation as shown in Figs 4, 5 and 7 is independent of the amount of coherency misfit.

5. CALCULATION OF THE CREEP STRAIN

5.1. *Overloading case*

Figure 9(a) shows the macroscopic creep strain in [001]-direction of the composite specimen versus normalize time. The strain rate increases rapidly in the first two time units staying constant there after. The steady state strain rate of the composite with cubic precipitates is 1/500 as compared to the steady state strain rate of the isolated matrix under the same load of 490 MPa. The value of the amount of coherency misfit δ^{coh} has only minor influence on the creep curves. The calculated and experimental creep curves coincide up to 0.5% plastic strain. After $\approx 0.5\%$ plastic strain the experimental strain rate accelerates and terminates the tertiary part, whereas our model remains in the stationary state. Alternating plates of γ and γ' phase as shown in Fig. 6 have half the strain rate than a morphology with γ' cubes.

5.2. *Underloading case*

Figure 9(b) shows the plastic elongation of specimens with cube or plate morphology during creep deformation under underloading conditions. Please notice the different time scale of $t_{norm} = 2 \cdot 10^6$ as

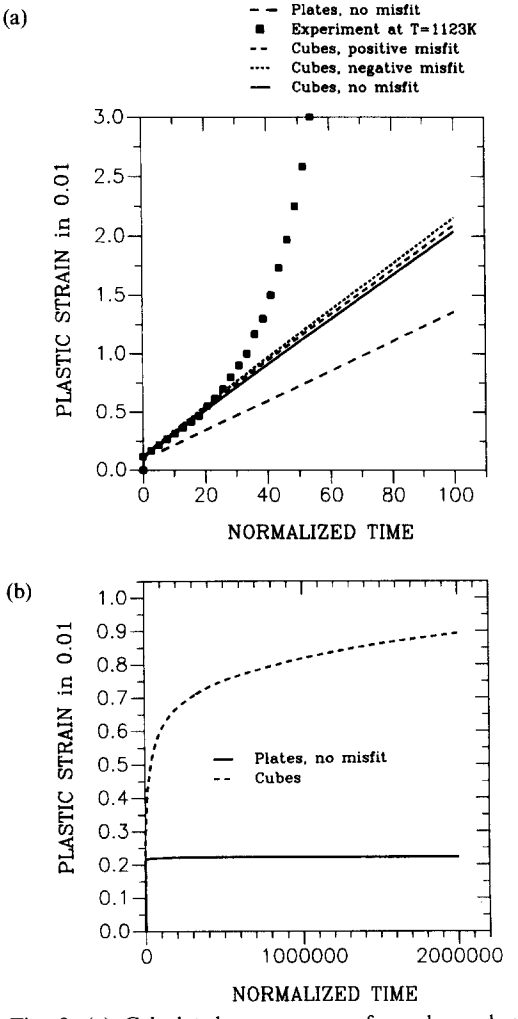

Fig. 9. (a) Calculated creep curves for cube and plate morphology for differential initial misfit values in overloading conditions. An experimental creep curve is shown for SRR99 at $T = 1123$ K under 490 MPa tensile load in [001] direction [19]. 100 normalized time units equal 430 h. (b) Calculated creep curves for the plate and cube morphology under underloading conditions. Note the larger time scale than in (a).

compared to Fig. 9(a) with $t_{norm} = 100$. Both creep curves asymptotically approach the strain rate zero. The deformation stops at a macroscopic plastic strain of 0.22% for the plate morphology and of 0.95% for the cube morphology.

5.3. Creep-induced lattice-mismatch of the plate morphology

During creep deformation the γ' morphology of negative misfit superalloys changes to a directionally coarsened raft-like structure perpendicular to the stress axis [16, 17]. Now we will discuss the amount of the creep-induced lattice mismatch in underloading conditions for the idealized plate-morphology of Fig. 6.

Formulas relating the stress and strain state with the coherency misfit were given in equations (2–8) [8] and equation (2) in [12]. Inserting the creep-induced lattice mismatch $\delta^{creep}_{parallel}$ parallel to the γ/γ' interface instead of δ^{coh}, one can utilize these formulas for our problem. The stationary creep-induced lattice mismatch parallel and perpendicular to the γ/γ' interface are then given by

$$\delta^{creep}_{parallel} = -\frac{(1-\nu)}{E \cdot V^{\gamma'}} \cdot \sigma_{ext} \tag{10}$$

$$\sigma^{creep}_{perpend} = \frac{-2\nu}{(1-\nu)} \cdot \delta^{creep}_{parallel}. \tag{11}$$

The Youngs' modulus E and Poissons' ratio ν are assumed to be equal for both phases. The equations are valid only for underloading conditions. $\delta^{creep}_{perpend}$ is the creep-induced lattice mismatch perpendicular to the phase interface. $V^{\gamma'}$ is the γ' volume fraction.

Under overloading conditions $\delta^{creep}_{parallel}$ and $\delta^{creep}_{perpend}$ depend linear on the equivalent γ' yield stress $\sigma^{\gamma'}_{yield}$. One can use formulas (10) and (11) for an overloading case by inserting $\sigma^{\gamma'}_{yield}$ instead of σ_{ext}.

In the same way, one can calculate the creep-induced lattice mismatch for plates (Fig. 6) under an [100] external load, parallel to the γ/γ' interface. The creep-induced lattice mismatch is zero in the [010] direction, perpendicular to the load axis. The lattice mismatch for [100] and [001] directions are given by equations (10) and (11) by replacing the factor $(1-\nu)$ with 1.

The total lattice mismatch δ^{total} is the sum of the creep-induced and coherency lattice mismatches.

6. COMPARISON WITH EXPERIMENT

6.1. X-ray analysis of creep-induced lattice parameter changes

The γ/γ' lattice mismatch of specimens of the monocrystalline nickel-base superalloy SRR99 was measured by X-ray diffraction after high temperature creep with different tensile loads [11, 13, 14]. The X-ray measurements were made at room temperature under zero load.

Figure 10 shows the experimental mismatch parallel (side case) and perpendicular (axial case) to the γ/γ' rafts after creep till rupture at 1323 K taken from [14]. The room temperature value of the coherency misfit $\delta^{coh} \approx -0.14\%$ was chosen for zero external load. The measured misfit depends linearly on the external creep load. The total axial misfit decreases with increasing creep load, whereas the side case misfit increases.

Making use of equations (10) and (11) for the underloading case (parameter set III) and the unconstrained coherency misfit value $\delta^{coh} \approx -0.2\%$ at 1323 K [12] we get the theoretical curves in Fig. 10 for the total lattice mismatch δ^{total}. Qualitatively, the theoretical calculations are able to describe the experimental measurements. However, the amount of the creep-induced lattice mismatch seems to be theoretically overestimated.

Two reasons for the discrepency between theoretical predicted and the measured lattice parameter changes will be discussed:

First, unloading the creep specimen, the von Mises stress level in the matrix increases from nearly zero up to the large value of $\sqrt{2} \cdot \sigma_{ext}$. Interfacial dislocations can combine to reduce the creep-induced misfit values.

Second, it was shown [22] that interfacial networks cannot completely compensate the von Mises stress level in the matrix as will be discussed further in Section 6.4.2.

Our FEM calculations show that under [001] load the creep-induced stress builds up within a macroscopic plastic deformation of 1% and remains nearly constant during further deformation. Indeed it was measured that during subsequent deformation the internal stress did not change significantly beyond 1.5% strain until rupture [14].

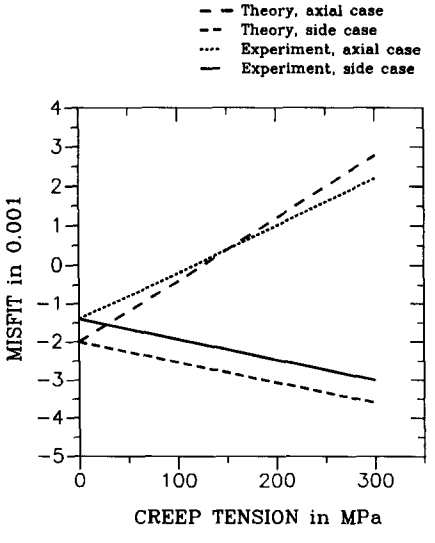

Fig. 10. Total γ/γ' lattice mismatch versus applied stress for the plate morphology crept at 1323 K. Measured values are taken from [14].

6.2. TEM investigations

6.2.1. Start of the matrix deformation. It has been observed that the deformation of negative misfit alloys starts in the horizontal matrix channels under [001] tensile load [7, 16] due to the high von Mises stress level as shown in Fig. 8. At later stages of deformation the plastic deformation also spreads in the other channels as predicted in Section 4.2.3.

6.2.2. Interfacial networks. Interfacial dislocation networks which build up during annealing or under creep load have been extensively studied [16–18]. The spacing d of the individual dislocations in these interfacial networks was correlated to the magnitude of the lattice mismatch by Brooks formula [26]

$$d = b/\delta \tag{12}$$

where b is the magnitude of the Burgers vector. Dislocation networks cannot compensate entirely the stresses in narrow matrix channels [22]. For matrix channels smaller than 100 nm and for our total misfit values Brooks formula must be modified [22]. However, in our continuum model the stress field in the matrix channels is permitted to relax totally. This deficit of our model can be avoided by introducing a modified creep law as will be done in Section 6.4.2.

As predicted in Section 4.2.3 an external load accelerates the formation of interfacial networks. At 1253 K the build-up of the neworks is finished after 500 h at zero load and after 40 h under 170 MPa [001] tensile load [16].

At high temperatures > 1123 K and under low load values directional coarsening occurs rapidly during primary creep and produces raft-like structures which remain essentially unchanged from the beginning of the secondary creep until late stages of deformation [16, 17]. After their formation during primary creep, the 60° and edge type dislocations remain stable during subsequent creep deformation [7, 16, 17]. Indeed, according to our calculations the build-up of the internal stresses in the microstructure was finished shortly after the primary creep.

The creep-induced interfacial dislocation spacing increases with decreasing creep load [20] according to equations (10) and (12). Also zero misfit alloys exhibit a finite creep-induced lattice spacing as measured [17] in accordance with Fig. 3(b).

The change of the sign of the Burgers vector relative to the phase interface from the horizontal to the vertical phase interface as shown in Figs 3(b) and 5(c) was observed [18].

Adding the dislocation networks caused by coherency misfit and creep-induced lattice mismatch for negative misfit alloys under tensile load, interfaces normal to the stress axis should be coated more densely by dislocations than those parallel to the exterior load [Fig. 3(c)]. The stationary mesh spacing of dislocation networks of SRR99 in the horizontal and vertical sections of the rafts were $d_{\text{horizontal}} \approx 60$ nm and $d_{\text{vertical}} \approx 90$ nm, respectively, under 170 MPa [001] tensile load [16]. In order to compare these experimental values with our theoretical considerations we use, for the sake of simplicity, Brooks formula of equation (12) and our idealized plate model for the horizontal and vertical matrix channels (see Section 5.3). We assume that the specimen is under underloading conditions.

Making use of the results in section 5.2 for the parameter set of SRR99 at 1253 K ($E = 82$ MPa, $\nu = 0.4$ [8, 23], $V^{\gamma'} = 0.68\%$ [24], $\delta_{\text{coh}} \approx -0.19\%$ [12]) one can predict the mesh spacings $d^{\text{horizontal}}_{\text{theoretical}} = 65$ nm, $d^{\text{vertical,[010]}}_{\text{theoretical}} = 132$ nm and $d^{\text{vertical,[001]}}_{\text{theoretical}} = 200$ nm. Considering the fact that it was experimentally not distinguished between $d^{\text{vertical,[010]}}_{\text{theoretical}}$ and $d^{\text{vertical,[001]}}_{\text{theoretical}}$, the theoretical values are in accordance with the measured ones.

6.2.3. Shearing of γ' cubes. Based on the von Mises stress distribution under [001] load as shown in Figs 4(a), 5(a) and 7 one would expect that the first matrix dislocation should enter the γ' cube near Point D where the γ' phase starts to flow. An example of such a penetration was shown in Fig. 17 in [7]. However, no systematic study have been made of the area where the matrix dislocations enter a γ' cube.

6.3. Creep curves

Figure 9(a) shows the comparison of an experimental curve compared with calculated ones for cubic γ' morphology. Up to a macroscopic plastic strain of 0.5% our theoretical creep curve follows the experimental one of SRR99 at 1173 K under 490 MPa [001] load. The stationary creep rate of the theoretical curve was made equal to the experimental one as discussed in Section 2.1. The macroscopic plastic strain where the experimental and theoretical curves leave the primary part is nearly equal in both cases. Up to a plastic strain of 0.5% the calculated creep strain decreases rapidly to a stationary value during subsequent deformation, whereas the experimental creep strain again increases during further deformation in the tertiary part.

Our model is strongly based on the compatibility of the two phases and cannot show creep mechanisms based on the total loss of coherency which seems to be important for the tertiary part of the creep curve [16, 20].

The (first) minimum creep rate $\dot{\epsilon}_{\text{min}}$ appears after strains lower than 1% [19, 20]. Our calculations show that the internal stresses are built up for macroscopic strains lower than 1%. It seems likely that the first minimum in the strain rate is related to the build-up of long-range internal stresses.

Our FEM calculations indicate that plates should have better creep properties than γ' cubes, especially under underloading conditions. The question, whether the presence of well-developed γ/γ' raft morphology has a beneficial or an adverse effect on the creep properties, has been discussed controversely [20, 27]. The problem in comparing the creep properties of cube and raft morphologies is that rafts can

only be produced by creep experiments at high temperatures. Then the creep properties of specimen with cubic morphology were compared with pre-rafted specimen at lower temperatures. According to the high experimental pre-deformation of 3% [20] compared to the lower plastic strains dealt with in our calculation (Fig. 9), a reliable comparison between the two morphologies, initial coherently embedded γ' plates and cubes, is not possible.

6.4. Estimation of γ' and γ yield stress in composite

Due to the small dimension and morphology of the microstructure, γ' and γ phases have different material parameters in composite as compared to the bulk states. Comparing experiments with our theoretical results one can estimate the material parameters of both phases in composite.

6.4.1. γ' yield stress. The linear dependence of the creep-induced lattice mismatch for raft structures versus applied stress from zero up to 300 MPa at 1323 K as shown in Fig. 10 indicates that the composite was under underloading condition for these parameters. Using the experimental values $\delta^{\text{creep}}_{\text{parallel}} \approx -0.16\%$ for $\sigma_{\text{ext}} = 300$ MPa at $T = 1323$ K (Fig. 5 in [13]) one might estimate utilizing equations (2), (10) and (11) for parameter set III

$$\sigma^{\gamma'}_{\text{yield},1323\,\text{K}} > \sigma_{\text{ext}} + \frac{E \cdot V^{\gamma}}{(1-\nu)} \cdot \delta^{\text{creep}}_{\text{parallel}} \approx 365\ \text{MPa}. \quad (13)$$

At 1033 K (SRR99, 750 MPa [001] load [28]) the γ' cube is cut by stacking faults even at an early stage of deformation, whereas at 1253 K and 170 MPa [001] tensile load the γ' rafts remained nearly dislocation free until shortly before rupture [16]. Therefore, according to our considerations in Section 4.2, the specimens were "overloaded" at 1033 K and "underloaded" at 1253 K. Making use of the definitions for the underloading and overloading case [equations (3) and (8)] one can estimate an upper and a lower bond for the yield stress of the γ' precipitate

$$\sigma^{\gamma'}_{\text{yield},1253\,\text{K}} > \sigma_{\text{ext}}/V^{\gamma'} = 170\ \text{MPa}/68\% = 250\ \text{MPa} \quad (14)$$

$$\sigma^{\gamma'}_{\text{yield},1033\,\text{K}} < \sigma_{\text{ext}}/V^{\gamma'} = 750\ \text{MPa}/70\% = 1070\ \text{MPa}. \quad (15)$$

The critical resolved shear stress of $Ni_3(Al, Ti)$ and the shear stress of γ' phase in composite were compared in Fig. 6 in [14]. The local shear stress in the γ' phase for the $\{111\}\ \langle\bar{1}01\rangle$ glide system is $\tau_{\text{critical}} = \sigma^{\gamma'}_{\text{yield}}/\sqrt{6}$. Our estimated lower bounds of τ_{critical} 149 MPa and 102 MPa at $T = 1323$ K fit roughly to the values presented in Fig. 6 in [14] where the critical resolved shear stress varied between 50 and 200 MPa at 1323 K depending on the strain rate. τ_{critical} varied between 300 and 470 MPa at 1033 K in Fig. 6 in [14] in accordance with our value of 437 MPa. It also approximately represents the critical resolved shear stress which is needed to produce antiphase boundaries in the γ' phase at lower temperatures [29].

6.5. Matrix yield stress

We assumed a simple creep-power law for the matrix phase in equation (1). Due to this creep law the coherency stress and the external load can be completely compensated in the underloading case during creep deformations as we see in Fig. 7.

However, theoretically it was shown [22] that the yield stress σ_0 of the γ phase forced into narrow matrix channels increases rapidly with decreasing channel size. The local von Mises stress level in the matrix channel must be greater than σ_0 in order to start matrix deformation. On the other hand σ_0 is also stress level in the small matrix channels, which cannot be relaxed by dislocation networks, which is demonstrated in [22].

Taking into account these two effects we can introduce a modified creep power law

$$\dot{\epsilon}_e = A \cdot (\sigma_{\text{Mises}} - \sigma_0)^n \quad (16)$$

where σ_0 is the threshold stress for the onset of matrix creep.

Using the modified creep law instead of the creep law of equation (1) our former calculations can be used further, if one transforms the external load σ_{ext} to $\sigma_{\text{ext}} - \sigma_0$ and the γ' yield stress $\sigma^{\gamma'}_{\text{yield}}$ to $\sigma^{\gamma'}_{\text{yield}} - \sigma_0$, respectively. Now the lowest possible value in the matrix channel is σ_0 during creep deformation under underloading conditions. General features of the threshold stress σ_0 have been discussed in [30]. We will propose three different options to get this important material data.

First, it is shown that creep curves can be better described with the creep law of equation (16) than with the simple law of equation (1) [19].

Second, by making use of the X-ray measurements of the lattice mismatch [13, 14] σ_0 is the difference between the von Mises stress values of the γ phase predicted by continuum mechanics, as done in Section 4, and the experimentally determined von Mises stress in the γ phase after creep deformation.

Third, one can calculate the threshold stresses σ_0 of the matrix by calculating the Orowan resistance that has to be overcome by dislocations moving through the matrix channel using the numerical program described in detail in [22]. The interfacial dislocations in nickel-base superalloys are created by dislocation gliding on octahedral planes through channels leaving 60° segments in the {001} interfaces as shown in Fig. 7 in [16, 22].

Utilising these three options one gets the equivalent σ_0-values of SRR99 to be 60, 67, and 70 MPa for a channel width of 160 nm at 1323 K, respectively.

7. SUMMARY

The stress and strain distributions in the microstructure of a two phase single crystal nickel-base

superalloy have been calculated after annealing and after creep in [001] direction using FEM and an elasto-plastic model.

Under zero load due to the lattice mismatch of the two phases the matrix channels are highly loaded while the channel crossings and the γ' phase are on low stress levels.

During long-term annealing under zero load the high coherency stresses in the matrix decrease drastically until a low stress level is reached for the whole microstructure.

A complex triaxial stress state builds up in the γ/γ' microstructure during creep. The von Mises stress level in the soft matrix decreases, whereas the stresses in the γ' precipitate can reach the γ' yield stress.

Two limiting cases can be distinguished: (i) the overloading case where during deformation the critical resolved shear stress is reached for the whole γ' volume, so that finally the material flows in total, (ii) the underloading case where the critical resolved shear stress is reached only at distinct and varying parts of the γ' particles.

The γ' plate morphology is predicted to have better creep properties than the γ' cube morphology. For the underloading conditions the critical resolved shear stress of the γ' phase is reached at no time during deformation.

Simulating creep deformation the long-range internal stresses were found to build up for plastic strains smaller than 1% and to remain constant during subsequent deformation. The coherency stresses are compensated at an early stage of creep deformation.

General features of the creep as the (first) minimum of the strain rate can be correlated with the build-up of internal stresses.

From the comparison of experimental results and theoretical predictions material parameters as the threshold stress σ_0 of the matrix and the yield stress of the γ' phase in composite can be obtained.

Acknowledgement—The authors are indebted to Deutsche Forschungsgemeinschaft for financial support (Sfb 339).

REFERENCES

1. T. M. Pollock and A. S. Argon, *Proc. Int. Conf. "Superalloy '88"*, Seven Springs, U.S.A., p. 285 (1988).
2. U. Glatzel and M. Feller-Kniepmeier, *Scripta metall.* **23,** 1839 (1989).
3. J. Gayda and R. A. MacKay, *Scripta metall.* **23,** 1835 (1989).
4. J. Gayda and D. J. Srolovitz, *Acta metall.* **37,** 641 (1989).
5. L. Müller, U. Glatzel and M. Feller-Kniepmeier, *Proc. Plasticity '91*, Grenoble, p. 512. Elsevier, Amsterdam (1991).
6. J. F. Ganghoffer, A. Hazotte, S. Denis and A. Simon, *Scripta metall.* **25,** 2491 (1991).
7. T. M. Pollock and A. S. Argon, *Acta metall.* **40,** 1 (1992).
8. L. Müller, U. Glatzel and M. Feller-Kniepmeier, *Acta metall.* **40,** 1321 (1992).
9. M. V. Nathal, R. A. MacKay and R. G. Garlick, *Mater. Sci. Engng* **75,** 195 (1989).
10. D. Bellet and P. Bastie, *Phil. Mag. B* **64,** 143 (1991).
11. H. A. Kuhn, H. Biermann, T. Ungar and H. Mugrabi, *Acta metall.* **39,** 2783 (1991).
12. L. Müller, T. Link and M. Feller-Kniepmeier, *Scripta metall.* **26,** 1297 (1992).
13. H. Biermann, A. Kuhn, T. Ungar and H. Mugrabi, *Proc. 9th Int. Conf. on Strength of Metals and Alloys*, Haifa, Vol. 1. Freund, London (1991).
14. H. Mugrabi, H. Biermann and T. Ungar, *Proc. 7th Int. Symp. on Superalloys*, Seven Springs (1992).
15. R. R. Keller, H. J. Mayer, H. Renner and H. Mugrabi, *Scripta metall. mater.* **27,** 1167 (1992).
16. M. Feller-Kniepmeier and T. Link, *Metall. Trans.* **20A,** 1233 (1989).
17. T. B. Gabb, L. Draper, D. R. Hull, R. A. MacKay and M. V. Nathal, *Mater. Sci. Engng* **A118,** 59 (1989).
18. R. R. Keller, H. J. Maier and H. Mugrabi, *Scripta metall.* **28,** 23 (1993).
19. T. Link and M. Feller-Kniepmeier, *Z. Metallk.* **80,** 152 (1989).
20. J. Hammer and H. Mugrabi, *Proc. First European Conf. on Advanced Materials and Processes*, Aachen, p. 449. DGM Informationsgesellschaft, Oberursel (1990).
21. A. A. Hopgood and J. Martin, *Mater. Sci. Technol.* **2,** 543 (1986).
22. G. Scheunemann-Freker, L. Müller and M. Feller-Kniepmeier, *Phil. Mag.* In press.
23. H. A. Kuhn and G. Sockel, *Physica status solidi* (a) **119,** 93 (1990).
24. R. Schmidt and M. Feller-Kniepmeier, *Scripta metall.* **26,** 93 (1992).
25. ABAQUS, Finite element program, Version 4.8. Hibibitt, Karlsson & Sorensen, R.I., U.S.A.
26. H. Brooks, *Metal Interfaces*, p. 20. Am. Soc. Metals, Metals Park, Ohio (1952).
27. M. V. Nathal, R. A. MacKay and R. V. Miner, *Metall. Trans.* **20A,** 133 (1989).
28. T. Link and M. Feller Kniepmeier, *Metall. Trans.* **23A,** 99 (1992).
29. M. Feller-Kniepmeier and G. Scheunemann-Frerker, *Phil. Mag.* **62,** 77 (1990).
30. P. J. Henderson and M. McLean, *Acta metall.* **31,** 1203 (1983).